Contrib Mineral Petrol (2002) 143: 664–672
DOI 10.1007/s00410-002-0375-4

Takehiko Hiraga · Osamu Nishikawa · Toshiro Nagase
Mizuhiko Akizuki · David L. Kohlstedt

Interfacial energies for quartz and albite in pelitic schist

Received: 14 January 2002 / Accepted: 10 May 2002 / Published online: 9 July 2002

Abstract Interfacial energies of quartz/quartz (qz/qz), albite/albite (ab/ab), and quartz/albite (qz/ab) boundaries in low-grade pelitic schist were determined based on measured values of dihedral angles. Three kinds of microstructures were investigated, and the interfacial energies were obtained in two independent ways. (1) Relative values of interfacial energy were calculated from dihedral angles formed at quartz and albite triple junctions. (2) Subgrain boundary energy was calculated using the Read–Shockley theory for a boundary connected to an intergranular pore. Dihedral angles formed at the corners of intergranular pores were measured. From the interfacial tension balance equation, the value of the qz/qz grain boundary energy was then obtained. (3) Dihedral angles formed at intersections of either pericline or albite twin boundaries with either ab/ab or qz/ab boundaries were measured. The twin boundary energy was calculated based on a previously derived equation using Landau potential, twin wall thickness, and critical temperature for a phase transition in albite. With a modified interfacial tension balance equation for a twin boundary fixed to a facet orientation, the interfacial energies of ab/ab and qz/ab boundaries were obtained. Energies obtained by methods of (2) and (3) are in good agreement. The interfacial energies for qz/qz, ab/ab, and qz/ab boundaries obtained in this study are 270 ± 110, 300 ± 150, and 250 ± 120 mJ/m^2, respectively.

T. Hiraga (✉) · D.L. Kohlstedt
Department of Geology and Geophysics,
University of Minnesota, Minneapolis,
MN 55455, USA
E-mail: hirag001@umn.edu

O. Nishikawa
Institute for Study of the Earth's Interior,
Okayama University at Misasa, Tottori, Japan

T. Nagase · M. Akizuki
Institute of Mineralogy,
Petrology and Economic Geology,
Faculty of Science, Tohoku University,
Aoba-yama, Aoba-ku, Sendai 980-8578, Japan

Editorial responsibility: T.L. Grove

Introduction

The interfacial free energy for solid grains in contact with one another (grain or phase boundary energy) directly affects grain boundary processes, such as grain boundary migration, fluid connectivity, grain boundary fracture strength, and grain boundary sliding, all processes that influence the dynamic behavior of the Earth's interior. However, except for the grain boundary energy of olivine in olivine-rich rocks (Cooper and Kohlstedt 1982; Duyster and Stöckhert 2001), grain and phase boundary energies of major minerals have not been determined.

The purpose of this paper is to determine interfacial energies for quartz and albite in natural rocks from their microstructures. Because segregation of impurities to grain and phase boundaries, as recently observed in synthetic aggregates of olivine (Hiraga et al., unpublished), can affect interfacial energy (e.g., Gleiter 1970), we emphasize this observation on natural rock samples.

Solutions for interfacial energies

Relative values of interfacial energies

In this study, we focused on the balance of interfacial tension at various triple junctions in pelitic schist. The dihedral angle, θ, provides a measure of the ratio of interfacial energies, γ_1 and γ_2, as expressed by the relation

$$2\cos(\theta/2) = \gamma_1/\gamma_2 \quad (1)$$

As an example, for a triple junction formed between two albite grains and a quartz grain in Fig. 1a, γ_1 and γ_2 correspond to the interfacial energies for a quartz/albite (qz/ab) phase boundary and an ab/ab grain boundary, respectively. Measured values for dihedral angles, θ, for qz vs. ab/ab and ab vs. qz/qz yield the relative values of interfacial energies for qz/qz, ab/ab

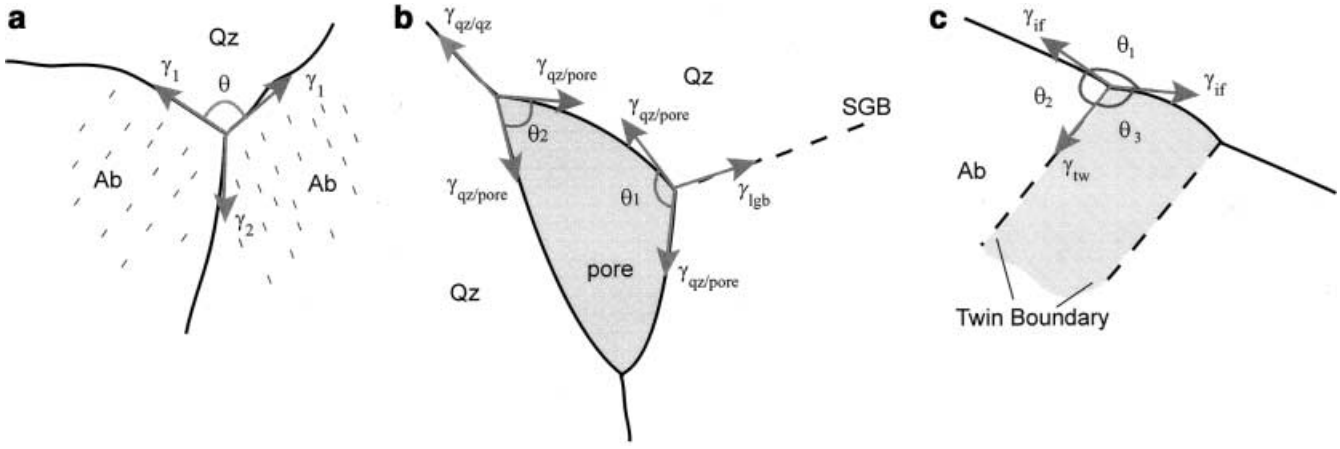

Fig. 1a–c. Schematic illustration of dihedral angles formed for various microstructures. **a** Dihedral angle formed at a triple grain junction by interfacial tension balance for two albite grains in contact with a quartz grain. **b** Dihedral angles formed at corners of an intergranular pore. The angles θ_1 and θ_2 are formed by interfacial tension balance at a subgrain boundary (SGB) in quartz and the pore, and at a grain boundary and the pore, respectively. **c** Dihedral angles formed at the intersection of a twin boundary and either an ab/ab or qz/ab boundary

and qz/ab boundaries. To obtain the absolute values of these interfacial energies, the interfacial energy of one of the boundaries was determined as described below.

Grain-boundary energy from the subgrain boundary connected to the intergranular pore

As one example, consider the case of a low-angle grain boundary (subgrain boundary) in a quartz grain intersecting an intergranular pore as illustrated in Fig. 1b. The energy of the low-angle grain boundary, γ_{lgb}, can be estimated from the Read and Shockley theory (Read and Shockley 1950) in terms of the misorientation between adjacent grains, ϕ. Hence, the quartz-pore interfacial energy, $\gamma_{\mathrm{qz/pore}}$, can be calculated from Eq. (1) with a measurement of θ_1, the dihedral angle between the pore and the quartz grains. In turn, the qz/qz grain boundary energy, $\gamma_{\mathrm{qz/qz}}$, can be calculated from Eq. (1) using this value for $\gamma_{\mathrm{qz/pore}}$ and the measured value for θ_2, the dihedral angle connected to high-angle (normal) grain boundary. Hiraga et al. (2001) have already reported a value of θ_2, as will be discussed below.

For a low-angle grain boundary with misorientation ϕ, γ_{lgb} is given by

$$\gamma_{\mathrm{lgb}}(\phi) = \gamma^0_{gb}\phi(A_0 - \ln\phi) \tag{2}$$

$$\gamma^0_{gb} = Kb/4 \tag{3}$$

where K is the appropriate elastic energy coefficient for the anisotropic medium and b is the length of the Burgers vector of the interfacial dislocations. A solution for K using the stiffness coefficients, C_{ij}, exists for a crystal if the line direction of the dislocations is parallel to an axis of rotational symmetry or normal to an axis of evenfold rotational symmetry (e.g., Hirth and Lothe 1982). Expressions for K have been calculated for some simple slip systems in low (α)-quartz (Heinisch et al. 1975). In addition, solutions for K for dislocations of arbitrary orientation can be obtained for hexagonal crystals (Teutonico 1970; Savin et al. 1976). Although the metamorphic condition of the sample used in this study was within the a-quartz stability field, we approximated the structure of quartz grains as that of high (β)-quartz (hexagonal) to obtain a relation between K and the C_{ij}'s for the slip system, a result that has not been calculated previously. We used published relationships derived for various types of dislocations in a hexagonal crystal (Teutonico 1970; Savin et al. 1976). In the dislocation coordinate system with the X_3 axis parallel to the dislocation and the X_2 axis in the basal plane, K is expressed as

$$K = \frac{1}{b^2}(K_{11}b_1^2 + K_{22}b_2^2 + K_{33}b_3^2 + 2K_{13}b_1b_3) \tag{4}$$

In this study, we specifically treat dislocations with Burgers vectors parallel to the basal plane ($b_2 = b$, $b_1 = b_3 = 0$). Thus, only K_{22} is required:

$$K_{22} = \frac{(b_0 + \rho)}{\mathrm{d}}[\delta_3 S_1 + S_2 d(d\delta_3 - \delta_1)] \tag{5}$$

where the symbols are elucidated in the Appendix. Values for the stiffness coefficients of $C_{11} = 117$, $C_{33} = 110$, $C_{44} = 36$ and $C_{13} = 33$ GPa at 600 °C were used (Hearmon 1984).

The term A_0 in Eq. (2) is related to the core energy of a dislocation and is expressed as

$$A_0 = 1 + \ln\frac{b}{2\pi r_0} \tag{6}$$

where r_0 is the radius of the dislocation core. Values of

$$\frac{b}{6} \le r_0 \le \frac{b}{2}$$

were used based on published values for KCl, NaCl, Ge, Al, MgO, and olivine (Wagner and Chalmers 1960; Hoagland et al. 1976; Woo and Puls 1977; Puls and So

1980; Tsurekawa et al. 1997; Duyster and Stöckhert 2001).

Interfacial energies from twin boundaries

As a second example, interfacial energies for ab/ab or qz/ab boundaries can be estimated from the dihedral angles formed at intersections with twin boundaries in albite, as illustrated in Fig. 1c. Because the structure of a twin boundary is usually well characterized, the dihedral angles θ_1, θ_2, and θ_3 formed at the junctions between twins and grain or phase boundaries can be used to determine the grain and phase boundary energies (King 1999). The twin boundary energy γ_{tw}, based on a Landau potential, is (Salje 1993)

$$\gamma_{tw} = \alpha \cdot W \cdot A \cdot T_c \tag{7}$$

where α is a prefactor, W the half-thickness of the twin wall, A a parameter related to the local effective potential, and T_c the temperature of the phase transition.

For an albite twin, boundary planes are limited to crystallographic planes such as (010). Thus, the direction of the twin boundary plane is fixed resulting in two different angles θ_2 and θ_3 in Fig. 1c. For this case, a corrected equation for interfacial tension balance is needed (King 1999):

$$\frac{\gamma_{if}}{\gamma_{tw}} = \frac{\sin(\theta_1/2)}{\sin\theta_1 \cdot \cos\left(\frac{\theta_1}{2} - \theta_{2\,\text{or}\,3}\right)} \tag{8}$$

Based on Eq. (8), γ_{if} can be calculated from the calculated value for γ_{tw}, and measured values of θ_1 and either θ_2 or θ_3.

Samples

Pelitic schist collected from the Asemi-gawa area in the Sanbagawa metamorphic belt in central Shikoku (e.g., Banno and Sakai 1989) was chosen for this study. Pelitic schists are widely distributed in this area, which is divided into four metamorphic zones: the highest metamorphic grade oligoclase–biotite zone, the albite–biotite zone, the garnet zone, and the lowest chlorite zone (Higashino 1990). The sample used in this study was collected from the chlorite zone. The sample is mainly composed of fine-grained (~30 μm) quartz, albite, chlorite, and muscovite. All of these minerals form grains elongated parallel to the foliation of the rock. The almost pure albite in the chlorite zone contains up to 0.5% An (e.g., Otsuki 1980), and twin boundaries are occasionally found. A TEM image of a typical region in this specimen is presented in Fig. 2. The peak metamorphic condition for this rock has been estimated to 250–300 °C at 500–600 MPa (Banno and Sakai 1989). The sample corresponds to the calcite-free pelitic schist of Hiraga et al. (2001). These authors reported the following TEM and Fourier-transform infrared spectroscopy (FTIR) results, which form essential information for this paper. (1) Nanometer-size intergranular pores are common at grain junctions. (2) The shape of most of the pores is determined by interfacial tension. (3) Subgrain boundaries often contain intergranular pores. (4) The water content in the sample as determined by FTIR shows that the observed pores were filled with an aqueous fluid. The fluid escaped from the pores during preparation of thin specimens for TEM. (5) Dislocations in quartz crystals were able to form and climb easily,

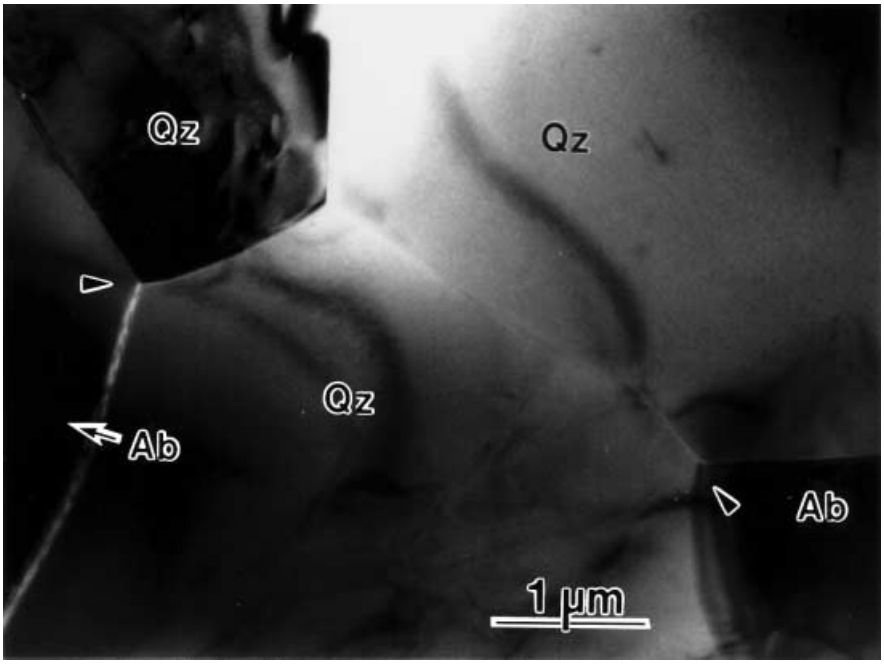

Fig. 2. TEM image of the pelitic schist. *Arrows* mark dihedral angles formed at ab vs. qz/qz

resulting in the formation of subgrain boundaries connected to the pores. Thus, at the time the pores formed, the temperature was greater than 200 °C, as required for quartz plasticity. (6) The dihedral angles formed at corners of the pores take a single value or at least narrow range of values. Although it is difficult to determine with which P–T condition the dihedral angles last equilibrated during cooling of the rock, the angles are comparable with the dihedral angle for the quartz–H_2O fluid system by Holness (1993) extrapolated to 250–300 °C and 400 MPa (7). The quartz–fluid dihedral angle changes with grain misorientation. As expected, the angle associated with a subgrain boundary is larger than the angle associated with a high-angle grain boundary because of the lower energy of subgrain boundaries.

Experimental procedure

To investigate the intergranular structure at the nanometer scale, the TEM was used for analyzing subgrain and twin boundaries, as well as for measurement for dihedral angles. Texture observations and chemical analyses were made with a 200-kV (JEM-2010) and a 300-kV (Philips CM30) electron microscope, both fitted with an energy dispersive X-ray analyzer (EDX). Crystallographic information was obtained from diffraction patterns. For measurements of dihedral angles, we aligned the axis of the triple junction as close as possible to parallel with the direction of incident electron beam. However, because of limitation of the rotation angle of the TEM specimen holder, this exact condition was not always met.

We used a reflected light microscope for dihedral angle measurements of ab vs. ab/ab. Observed angles are different from the real ones; however, the median of the observed angles corresponds to the true angle, if the samples have a single dihedral angle (Riegger and Van Vlack 1960). Polished sections were chemically etched with a HF solution to distinguish quartz from plagioclase and to highlight the interfaces. To get statistically accurate angles, a large number ($n \sim 200$) of angles were measured by this method.

Results

Dihedral angles at triple junctions

Distributions of dihedral angles for ab vs. ab/ab, qz vs. ab/ab and ab vs. qz/qz are shown in Fig. 3a–c. With TEM, the angles can be measured with high-resolution; however, the numbers of angles that can be measured is very limited because we can only observe a very small region in the specimen. Consequently, for qz vs. ab/ab and ab vs. qz/qz, the number of measured angles is small. The peak and the median angles for ab vs. ab/ab are similar with a value of ~120°. Both angle distributions

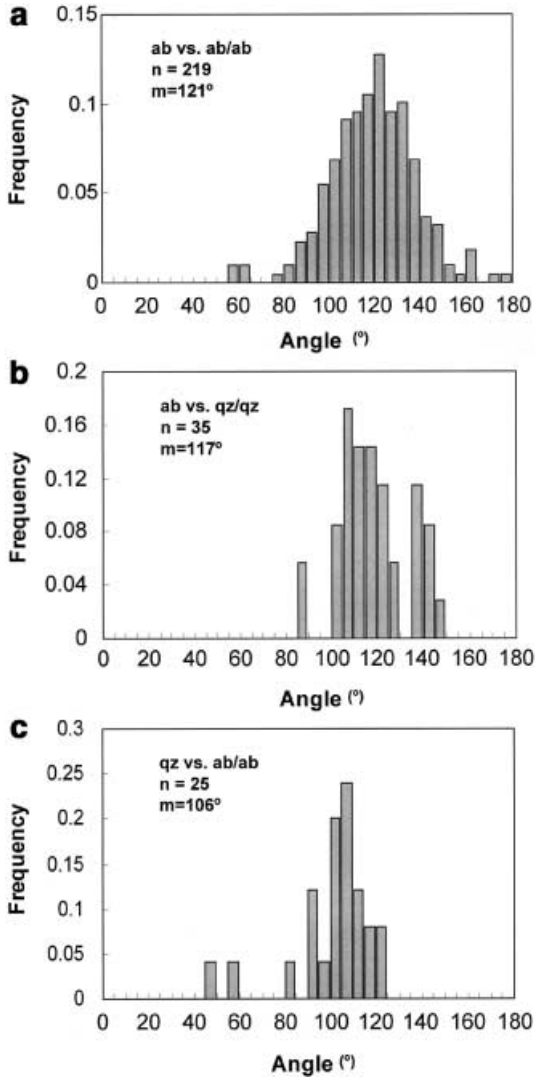

Fig. 3a–c. Distributions of dihedral angle formed at triple junctions. **a** Ab vs ab/ab angles measured on a reflected light optical microscope images. *n* Number of measured angles; *m* median of the measured angles. **b** Ab vs. qz/qz measured on TEM images. **c** Qz vs. ab/ab measured on TEM images

in qz vs. ab/ab and ab vs. qz/qz have distinct peaks; however, the peak and the median angles are slightly different, possibly because of the limited number of measurements or to crystal anisotropy.

Subgrain boundary analysis by TEM

Some subgrain boundaries in quartz grains are connected to intergranular pores (i.e., fluid inclusions). To determine the interfacial energy, a simple subgrain boundary in contact with intergranular fluid inclusions was analyzed. In Fig. 4a, a periodically aligned set of dislocations forms a subgrain boundary in a quartz grain. In the image, dislocations are observed as points, especially in the thin region near the sample edge because they are almost parallel to the incident electron

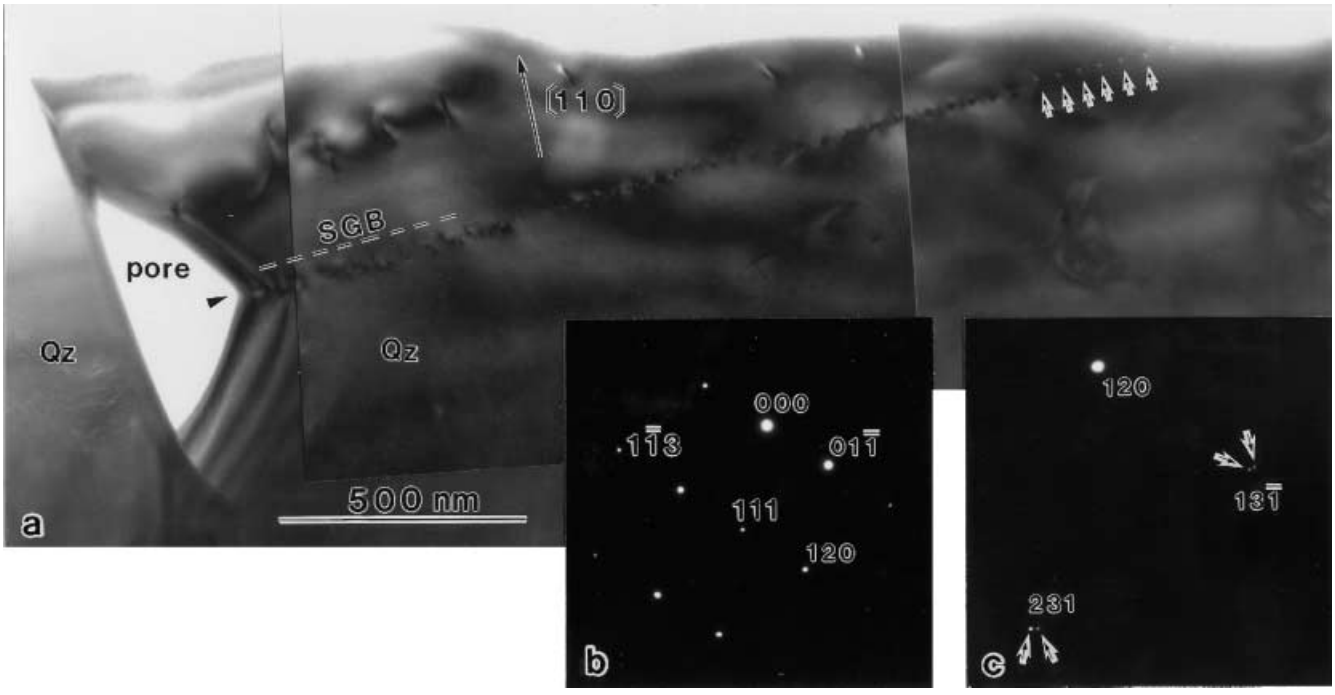

Fig. 4a–c. TEM image and diffraction patterns taken with the incident beam parallel to $[2\bar{1}\bar{1}]$. **a** Periodic aligned dislocations indicated by a *row of arrows* form a subgrain boundary (SGB) connected to a *triangular pore*. *Arrow* in the pore shows dihedral angles between the pore and the quartz grain. **b** Diffraction pattern from the region of the subgrain boundary. **c** Enlargement pattern of **b**. Pairs of diffraction spots pointed by *arrows* indicate that the regions separated by the boundary are misoriented by $0.7 \pm 0.1°$

beam. Dislocations in the boundary are separated by a constant interval of ~44.4 nm, demonstrating that the subgrain boundary is formed with one type of dislocation. The boundary intersects to a pore with symmetrically curved grain faces. The dihedral angle at the corner of the pore connected to the boundary is $130 \pm 1°$. The plane of the subgrain boundary is almost parallel to the {120} plane and perpendicular to the $\{1\bar{1}3\}$ plane of quartz. Because our TEM analysis cannot treat quartz as a trigonal crystal, but as a hexagonal crystal, these crystallographic numbers are for hexagonal symmetry. Two pairs of diffraction spots in Fig. 4c show that adjacent grains are misoriented by $0.7 \pm 0.1°$ around a rotation axis almost parallel to $[2\bar{1}\bar{1}]$.

Twin boundary analysis by TEM

Twin boundaries were observed in albite grains. At the intersection of a twin boundary with an ab/ab or qz/ab boundary, the grain or phase boundary is slightly curved, indicating a balance of twin and grain/phase boundary tension as shown in Fig. 5. The type of twin, either albite or pericline, can be determined from diffraction patterns. For example, based on the diffraction pattern in Fig. 5, the boundary plane is parallel to (010) of albite, consistent with an albite twin. There are fewer pericline twins than albite twins in the sample; thus, one pericline twin and five albite twins were analyzed. Measured values of dihedral angles and calculated values of interfacial energies are summarized in Table 1. As shown in Fig. 1c, we collected three angles at each twin and grain/phase boundary intersection. Some of the intersections are not concave so that $\theta_1 = 180°$. This situation indicates that interfaces correspond to low-index crystallographic planes of quartz or albite that fail to develop interfacial tension balance at the intersections. We did not include this type of structure in the angle measurements. Most twin boundaries are not orthogonal to grain and phase boundaries, thus yielding two different values for both θ_1 and θ_2. Although the number of measured angles is small, θ_1 does not depend significantly on the type of twin or the types of intersecting interfaces, and θ_1 is very large, $174.5 \pm 1.5°$.

Discussion

Relative interfacial energies

The quartz and the albite grains are elongated parallel to the foliation of the rock, indicating that the shape of the grains is not entirely controlled by the minimization of interfacial energy. At low-temperature conditions, interfaces cannot migrate enough to minimize interfacial energies. However, at many triple junctions, the interfaces are curved as demonstrated in Fig. 2. The interfaces appear to have locally rearranged to balance interfacial tension at each triple junction. This supposition is supported by the measurement of the dihedral angles at triple junctions of albite grains as shown in Fig. 3a. Although the observed dihedral angles do not

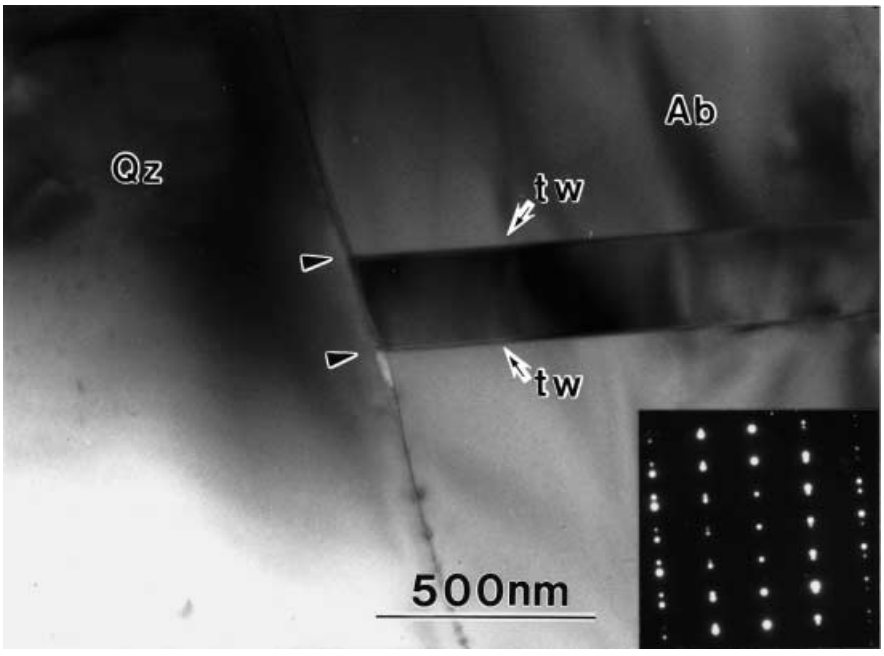

Fig. 5. TEM image of intersections of twin boundaries and qz/ab phase boundary plus diffraction pattern from one of the twin boundaries. The *arrows* identify the dihedral angle θ_1 formed at the intersections. Based on diffraction pattern analysis, type of the twin (*tw*) is characterized as albite twin, whose boundary plane is parallel to (010)

Table 1. Measured values of dehedral angles and calculated values of interfacial energies for albite and pericline twin boundaries

Twin type	Interface type	θ_1 (°)	θ_2 (°)	θ_3 (°)	γ_{if}/γ_{tw}	γ_{if} (mJ/m^2)
Pericline	Ab/Ab	174	94	92	9.5	161
Albite	Qz/Ab	176	88.5	95.5	14.0	238
Albite	Qz/Ab	174	93	93	9.5	161
Albite	Ab/Ab	175	101	84	11.6	197
Albite	Qz/Ab	173	107	80	8.6	147
Albite	Qz/Ab	176	78	106	14.2	242

exhibit the predicted distribution for random planar sections in three-dimensional samples with a single dihedral angle (Jurewicz and Jurewicz 1986), both the peak and the median of the angle distribution are ~120°, the value expected for the balance of interfacial tensions at a triple grain junction. Thus, we suggest that the medians or/and peaks of other observed angle distributions coincide with true angles. Additionally, previously reported values for quartz–feldspar dihedral angles are similar to our values, even though the metamorphic conditions are very different (Vernon 1968; Hiraga 1999; Holness and Clemens 1999). Including small differences between the peak and the median angles in Fig. 3b, c, for ab vs. qz/qz and for qz vs. ab/ab, we use dihedral angles of $111 \pm 6°$ and $107 \pm 3°$, respectively, to calculate relative interfacial energies. Consequently, the ratio $\gamma_{qz/qz}:\gamma_{ab/ab}:\gamma_{qz/ab} = 1:1.06 \pm 0.12:0.89 \pm 0.07$ is obtained.

Structure of subgrain boundary

The slip systems of quartz at various conditions and the dislocations forming subgrain boundaries have previously been characterized (e.g., Baëta and Ashbee 1969; Trépied et al. 1980). To reduce the strain energy in grains caused by free dislocations, the dislocations organize into subgrain boundaries parallel to a specific plane that tends to be normal to slip planes. Thus, in the observed structure in Fig. 4a, the $<110>$ slip direction, which is tilted 11° from $<120>$, is the only appropriate slip direction among the well-studied slip systems in quartz (e.g., Baëta and Ashbee 1969; Trépied et al. 1980). The $\{1\bar{1}3\}$ plane is almost perpendicular (~86°) to the subgrain boundary plane and parallel to the Burger's vector of the dislocations. Therefore, dislocations belonging to $\{1\bar{1}3\}<a>$ slip system are the most appropriate constituents for the subgrain boundary. Although this slip system has not been commonly reported (e.g., Baëta and Ashbee 1969), Nishikawa and Takeshita (2000) showed that the crystallographic orientations of subgrains and recrystallized grains in quartz veins collected from the same metamorphic belt as the present sample are explained by the same $\{1\bar{1}3\}<a>$ slip system (correspond to $\omega\{103\}<a>$ in their paper). Basal $(001)<a>$ slip, the most common slip system in quartz, specifically develops at low temperatures similar to those experienced by this rock. Lattice preferred orientation data for quartz in a schist, collected from the

same area as the present sample, exhibits a cleft girdle type and a type I cross girdle (Tagami and Takeshita 1998) resulting from primary slip on the system (001)<a> (Lister et al. 1978). Although an ideal dislocation from the (001)<a> slip system is inclined at ~25° to the incident electron beam direction, the possibility of the dislocations belonging to the basal slip system remains. The length of the Burgers vector (b) can be calculated from the relation $\phi = b/h$, where h is the spacing between dislocations. With $\phi = 0.7 \pm 0.1°$ and $h = 44.4$ nm, $b = 0.54 \pm 0.08$ nm, which is in good agreement with the length of the a-axis of quartz. This result is consistent with observations from previous studies (e.g., Trépied et al. 1980; Mclaren et al. 1989).

Estimation of grain boundary energy for qz/qz boundaries from subgrain boundary structure

The dihedral angle for intergranular pores connected to high-angle grain boundaries in quartz is $45 \pm 5°$, the value derived from the distribution of observed dihedral angles (Hiraga et al. 2001). In contact with the subgrain boundary, the dihedral angle is $130 \pm 1°$. Substitution of these values into Eq. (1) yields $\gamma_{lgb}:\gamma_{gb} = 1:2.2 \pm 0.1$.

For a dislocation on the basal plane with $\boldsymbol{b} = (1/3)$<a>, $K = 45$ GPa at 25 °C and $K = 44$ GPa at 500 °C (Heinisch et al. 1975). Further, for a dislocation on the $\{1\bar{1}3\}$ plane with $\boldsymbol{b} = (1/3)$<a>, $K = 44$ GPa at 600 °C based on Eq. (4). Heinisch et al. (1975) showed that the value of K decreases by <10 GPa in various <a> slip systems from room temperature to 550 °C near the α–β transition. Therefore, calculation of K for the $\{1\bar{1}3\}$<a> slip system based on Eq. (4) gives lower values. Taking these factors into consideration, the subgrain boundary energies including both the $\{1\bar{1}3\}$<a> and the (001)<a> cases are estimated using Eq. (2) with $b = 0.49$ nm for α-quartz and $K = 50 \pm 5$ GPa. Substitution of these values into Eqs. (2) and (3) yields $\gamma_{lgb} = 120 \pm 45$ mJ/m^2. Consequently, γ_{gb} (qz/qz) $= 270 \pm 110$ mJ/m^2. Also, the interfacial energy for quartz in contact with an aqueous fluid is $\gamma_{qz/pore} = 145 \pm 55$ mJ/m^2 from Eq. (1).

Interfacial energies for pl/pl and qz/pl boundaries from twin boundary structure

Because the sample used for twin boundary analysis did not experience a metamorphic event higher above the phase transition for albite, that is, low-albite to high albite, the twins might have formed by glide twinning during deformation (e.g., Lawrence 1970; Olsen and Kohlstedt 1985). It is known that albite and pericline twins are the only twins that can be formed by glide. Olsen and Kohlstedt (1985) showed that pericline twins are less numerous than albite twins in plagioclase from a shear zone, a feature consistent with our observations. Hayward et al. (1996) measured a width of $2W = 2.5 \pm 0.1$ nm for pericline twin walls from diffuse X-ray diffraction caused by the walls. As suggested by Hayward and Salje (2000), the width of albite twin walls is likely to be similar to the width of pericline twin walls because their formation process at a phase transition and displacement of the lattice are similar. In addition, no significant difference in dihedral angle (θ_1) is observed between the two types of twin (Table 1). Thus, we use the thickness of a twin wall of 2.5 ± 0.1 nm not only for pericline twins, but also for albite twins. T_c changes significantly with orthoclase content above ~3%, but is stable at $T_c = 1{,}327$ K for 0 to ~3% orthoclase (Hayward and Salje 1996), the concentration in our albite grains. Chrosch and Salje (1999) and Salje (2000) use $\alpha = 1/8$ as a conservative value for twins in various materials (Salje and Hayward personal communication). With $A = 8.23$ J/mol·K for pure albite referred in Hayward and Salje (1996), $\alpha = 1/8$, $T_c = 1{,}327$ K and $2W = 2.5 \pm 0.1$ nm, a value of $\gamma_{tw} = 17 \pm 1$ mJ/m^2 is obtained from Eq. (7) for both types of twins. Using Eq. (8), measured values of θ_1, θ_2, and θ_3, and the twin boundary energy yields $\gamma_{if} = 205 \pm 65$ mJ/m^2; this range includes interfacial energies of both ab/ab grain boundaries and qz/ab phase boundaries (Table 1). This result is in good agreement with interfacial energies for ab/ab and qz/ab boundaries determined above from qz/qz grain boundary energy with relative interfacial energies for them.

Comparison with interfacial energies in different systems

As shown above, two independent methods give almost the same value for the interfacial energies. We propose interfacial energies for qz/qz boundaries of 270 ± 110 mJ/m^2, for ab/ab boundaries of 300 ± 150 mJ/m^2, and for qz/ab boundaries of 250 ± 120 mJ/m^2, which include values determined by different methods. The ranges may be small enough for practical application to geological phenomena such as grain growth, fluid distribution, and microtexture formation in rocks (e.g., Jurewiscz and Watson 1984; Urai et al. 1986; Masuda et al. 1997). As discussed previously, these energies are obtained from the microstructures equilibrated at lower than 300 °C and 600 MPa, which is the highest metamorphic condition that the rock experienced.

The present values for interfacial energies are relatively small compared with values reported for other materials. For example, grain boundary energies for NiO and MgO are estimated to be ~3,000 mJ/m^2 (Duffy and Tasker 1983). Also, grain boundary energy of olivine is estimated to be 900 ± 350 mJ/m^2 (Cooper and Kohlstedt 1982) and ~1,400 mJ/m^2 (Duyster and Stöckhert 2001); this difference maybe because of the difference in temperature with which their samples last equilibrated. Holness (1992, 1993) suggested that the quartz grain boundary and quartz–H_2O fluid interfacial energies decrease with increasing temperature and

pressure in the low temperature regime (up to 600 °C at constant pressure of 400 MPa) and in the low pressure regime (up to 600 MPa at constant temperature of 800 °C) in quartz–H_2O fluid systems. Because intergranular aqueous fluid inclusions are numerous in our rock sample, water must have been abundant and maybe comparable to the hydrous environment at the experimental conditions. Therefore, the values of interfacial energy obtained in this study should represent relatively high values for interfacial energies for rocks from the Earth's crust because our values must reflect conditions less than or equal to the highest metamorphic condition that the rock experienced. Our value for quartz–aqueous fluid interfacial energy (145 ± 55 mJ/m^2) can be compared with the interfacial energy of quartz–liquid water (335–385 mJ/m^2) determined at ambient conditions (Parks 1984), again taking into account the observation that the energy decreases with increasing temperature and pressure.

Acknowledgements This research was funded by a JSPS Postdoctoral Fellowship for Research Abroad and the NSF through grant EAR-0126277. E.L.K. Salje and S.A Hayward are gratefully acknowledged for the derivation of the twin boundary energy. We thank M. Shiba for helping to collect our samples. M. Holness and an anonymous reviewer are acknowledged for helpful and constructive comments.

Appendix

$$S_1 = \frac{b_0^2(g\,\cos^4\Theta + \delta_{13}\delta_3^4}{2k(b_0+\rho)^2}$$

$$S_2 = \frac{4b_0^2\delta_3^2\cot^2\Theta}{(b_0+\rho)^2}$$

$$\delta_1^2 = \frac{k + l\,\sin^2\Theta - m\,\sin^4\Theta}{k}$$

$$\delta_2 = \frac{2k + l\,\sin^2\Theta}{k}$$

$$\delta_3^2 = \frac{b_0 + \rho\,\sin^2\Theta}{b_0}$$

$$d = \frac{1}{2}\sqrt{\delta_2 + 2\delta_1}$$

$$b_0 = C_{66}$$

$$\rho = C_{44} - C_{66}$$

$$k = C_{11}C_{66}$$

$$l = (C_{11}C_{33} - C_{13}^2) - 2C_{44}(C_{11} + C_{13})$$

$$m = (C_{11}C_{33} - C_{13}^2) - C_{44}(C_{11} + C_{33} + 2C_{13})$$

$$\delta_{13} = C_{11}C_{33} - C_{13}^2$$

$$g = C_{11}C_{33} - (C_{13} + 2C_{44})^2$$

Θ: angle between c axis and a dislocation line

$\left(\Theta = 67^\circ \text{ for } \{1\,\bar{1}\,3\}, b = (1/3)\langle 1\,10\rangle \text{ slip system}\right)$.

References

Baëta RD, Ashbee KHG (1969) Slip systems in quartz: I. experiments. Am Mineral 54:1551–1573

Banno S, Sakai C (1989) Geologic and metamorphic evolution of the Sanbagawa metamorphic belt, Japan. In: Daly JS et al. (eds) Evolution of metamorphic belts. Geol Soc Spec Publ 43:519–532

Chrosch J, Salje EKH (1999) Temperature dependence of the domain wall width in $LaAlO_3$. J Appl Phys 85:722–727

Cooper RF, Kohlstedt DL (1982) Interfacial energies in the olivine–basalt system. In Akimoto S, Manghnami MH (eds) High pressure research in geophysics. Adv Earth Planet Sci 12:217–228

Duffy DM, Tasker PW (1983) Properties of grain boundaries in rock salt structured oxides. In Kingery WD (ed) Advances in ceramics, vol 10 (structure and properties of MgO and Al_2O_3 ceramics). American Ceramic Society, Columbus, Ohio, pp 275–289

Duyster J, Stöckhert B (2001) Grain boundary energies in olivine derived from natural microstructures. Contrib Mineral Petrol 140:567–576

Gleiter H (1970) The segregation of copper at high angle grain boundaries in lead. Acta Metall 18:117–121

Hayward SA, Salje EKH (1996) Displacive phase transition in anorthoclase: the "plateau effect" and the effect of T1–T2 ordering on the transition temperature. Am Mineral 81:1332–1336

Hayward SA, Salje EKH (2000) Twin memory and twin amnesia in anorthoclase. Mineral Mag 64:195–200

Hayward SA, Chrosh J, Salje EKH, Carpenter MA (1996) Determination of the thickness of twin walls in anorthoclase: an X-ray diffraction study. Eur J Mineral 8:1301–1310

Hearmon RFS (1984) The elastic constants of crystals and other anisotropic materials. In: Hellwege KH, Hellwege AM (eds) Landolt–Börnstein tables, vol III/18. Springer, Berlin Heidelberg New York

Heinisch HL, Sines G, Goodman JW, Kirby SH (1975) Elastic stresses and self-energies of dislocations of arbitrary orientation in anisotropic media: olivine, orthopyroxene, calcite, and quartz. J Geophys Res 80:1885–1896

Higashino T (1990) Metamorphic zones of the Sambagawa metamorphic belt in central Shikoku, Japan (in Japanese with English abstract). J Geol Soc Jpn 96:703–718

Hiraga T (1999) Interface structure and interfacial energy in metamorphic rocks studied by electron microscopy. PhD Thesis, Tohoku University, Sendai

Hiraga T, Nishikawa O, Nagase T, Akizuki M (2001) Morphology of intergranular pores and wetting angles in pelitic schists studied by transmission electron microscopy. Contrib Mineral Petrol 141:613–622

Hirth JP, Lothe J (1982) Theory of dislocations. Wiley, New York

Hoagland RG, Hirth JP, Gehlen PC (1976) Atomic simulation of the dislocation core structure and Peierls stress in alkali halide. Philos Mag 34:413–439

Holness MB (1992) Equilibrium dihedral angles in the system quartz–CO_2–H_2O–NaCl at 800 °C and 1–15 kbar: the effects of pressure and fluid composition on the permeability of quartzites. Earth Planet Sci Lett 114:171–184

Holness MB (1993) Temperature and pressure dependence of quartz-aqueous fluid dihedral angles: the control of absorbed H_2O on the permeability of quartzites. Earth Planet Sci Lett 117:363–377

Holness MB, Clemens JD (1999) Partial melting of the Appin Quartzite driven by fracture-controlled H_2O infiltration in the aureole of the Ballachulish Igneous Complex, Scottish Highlands. Contrib Mineral Petrol 136:154–168

Jurewicz SR, Jurewicz AJG (1986) Distribution of apparent angles on random sections with emphasis on dihedral angle measurements. J Geophys Res 91:9277–9282

Jurewicz SR, Watson EB (1984) Distribution of partial melt in a felsic system: the importance of surface energy. Contrib Mineral Petrol 85:25–29

King AH (1999) Twin intersections with grain boundaries. In: Ankem S, Pande CS (eds) Advances in twinning. The Minerals, Metals and Materials Society, Warrendale, PA, pp 287–299

Lawrence RD (1970) Tectonic significance of petrofabric studies along the Chewack–Pasayten fault, north-central Washington. Geol Soc Am Bull 89:731–743

Lister GS, Paterson MS, Hobbs BE (1978) The simulation of fabric development in plastic deformation and its application to quartzites: the model. Tectonophysics 45:107–158

Masuda T, Morikawa T, Nakayama Y, Suzuki S (1997) Grain-boundary migration of quartz during annealing experiments at high temperatures and pressures, with implications for metamorphic geology. J Metamorph Geol 15:311–322

Mclaren AC, FitzGerald JD, Gerrestsen J (1989) Dislocation nucleation and multiplication in synthetic quartz: relevance to water weakening. Phys Chem Minerals 16:465–482

Nishikawa O, Takeshita T (2000) Progressive lattice misorientation and microstructural development in quartz veins deformed under subgreenschist conditions. J Struct Geol 22:259–276

Olsen TS, Kohlstedt DL (1985) Natural deformation and recrystallization of some intermediate plagioclase feldspars. Tectonophysics 111:107–131

Otsuki M (1980) Notes on petrography and rock-forming mineralogy (7) Zonal structure of albite porphyroblast from basic Sanbagawa schists in central Shikoku. J Jpn Assoc Mineral Petrol Econ Geol 75:196–202

Parks GA (1984) Surface and interfacial free energies of quartz. J Geophys Res 89:3997–4008

Puls MP, So CB (1980) The core structure of an edge dislocation in NaCl. Phys Stat Sol (b) 98:87–96

Read WT, Shockley W (1950) Dislocation models of crystal grain boundaries. Phys Rev 78:275–289

Riegger OK, Van Vlack LH (1960) Dihedral angle measurement. AIME Trans 218:933–935

Salje EKH (1993) Phase transitions in ferroelastic and coelastic crystals, 2nd edn. Cambridge University Press, Cambridge

Salje EKH (2000) Ferroelasticity. Contemp Phys 41:79–91

Savin MM, Chernov VM, Strokova AM (1976) Energy factor of dislocations in hexagonal crystals. Phys Stat Sol 35:747–754

Tagami M, Takeshita T (1998) C-axis fabrics and microstructures in quartz schist from the Sambagawa metamorphic belt central Shikoku Japan. J Struct Geol 20:1549–1568

Teutonico LJ (1970) Dislocations in hexagonal crystals. Material Sci Eng 6:27–47

Trépied L, Doukhan JC, Paquet J (1980) Subgrain boundaries in quartz. Theoretical analysis and microscopic observations. Phys Chem Minerals 5:201–218

Tsurekawa S, Morita K, Nakashima H, Yoshinaga H (1997) Geometric structures of grain boundaries expected from the O-lattice theory compared with high-resolution transmission electron microscope images. Trans Jpn Inst Mater 38:393–400

Urai JL, Means WD, Lister GS (1986) Dynamic recrystallization of minerals. Am Geophys Union, Geophys Monogr 36:161–199

Vernon RH (1968) Microstructures of high-grade metamorphic rocks at Broken Hill, Australia. J Petrol 9:1–22

Wagner RS, Chalmers B (1960) Grain boundaries in germanium. J Appl Phys 31:581–587

Woo CH, Puls MP (1977) Atomistic breathing shell model calculations of dislocation core configurations in ionic crystals. Phil Mag 35:727–756